Lowland Technology International 2016; 18 (1): 9-22
International Association of Lowland Technology (IALT): ISSN 1344-9656

Research Paper

Effect of Boundary Conditions in Segmental Lining Model on its Sectional Force

S. Chaiyaput [1] and M. Sugimoto [2]

ARTICLE INFORMATION

Article history:

Received: 14 April, 2016
Received in revised form: 29 May, 2016
Accepted: 31 May, 2016
Publish on: June,2016

Keywords:

Shield tunneling method
Segment
3D FEM
Boundary condition
Sectional force.

ABSTRACT

Nowadays, underground construction becomes popular as the demand for infrastructure in urban areas increases. To develop underground space in an urban area, it is important to investigate ground surface settlement and damage to existing neighbouring structures. Consequently, 3D finite element method (FEM) continuum models have been developed. This paper introduces a 3D FEM continuum model, which can consider, longitudinal joints, circumferential joints, and non-tension boundary between lining and ground, and examines the effect of boundary condition at the tunnel end and ground stiffness on the lining behavior (i.e., bending moment, axial force, normal effective earth pressure, and segment displacement) in the case of staggered building. As a result, it was found that the boundary condition at the tunnel end does not significantly affect the sectional force, except for the axial force in the case of soft soil; The two-ring model provides the safe side results from the viewpoint of segment design; and it can be adopted for segmental lining design and lining behavior simulation.

1. Introduction

The demand for infrastructure projects in urban areas, such as buildings, highways, railroads, and waterways, increases nowadays. Due to the limitation of land area, underground space use has become one alternative. Recently, shield tunnelling is the major tunnel construction method for the urban area on soft ground because this method minimizes ground disturbance and also influence to existing building above the construction area. The shield tunnel lining shown in Fig. 1 is assembled by connecting cylindrically shaped rings, which are composed of some segments. In the segmental lining design (ITA working group. 2000), the modified usual calculation method (Murakami and Koizumi, 1978; JSCE, 1996) was commonly used previously. This method is a one-ring model in which the lining is modelled by a curved beam without joints, as shown in Fig. 2(a). Here, longitudinal joints and circumferential joints are evaluated by the effective rate of bending stiffness and the increment rate of bending moment instead of modelling joints. The interaction between lining and ground is counted by the ground reaction force around the spring line. Recently, 2D beam-spring models (e.g., JSCE, 1996; Lam et al., 2014) have become common. As shown in Fig. 2(b), the model consists of two segmental rings under 2D strain condition, since the longitudinal joint position is by turns for odd number ring and even number ring in case of staggered building. The lining is modelled by beam elements; the longitudinal joint and circumferential joint are represented by a rotation spring and a shear spring in radial and

[1] Graduate student, Department of Civil and Environmental Engineering, Nagaoka University of Technology, 1603-1 Kamitomioka, Nagaoka, Niigata 940-2188, JAPAN, salisa.fern@gmail.com
[2] Professor, Department of Civil and Environmental Engineering, Nagaoka University of Technology, 1603-1 Kamitomioka, Nagaoka, Niigata 940-2188, JAPAN, sugimo@vos.nagaokaut.ac.jp
Note: Discussion on this paper is open until September 2016.

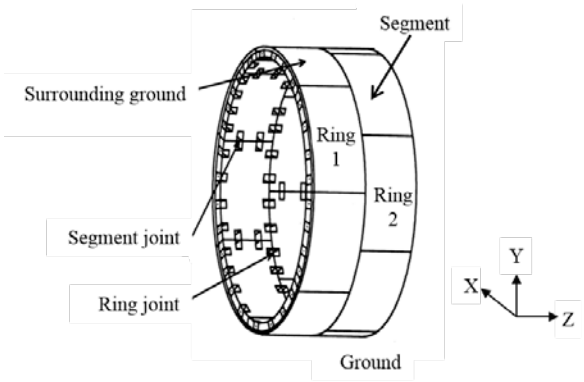

Fig. 1. Shield tunnel lining components. (JTA, 2000)

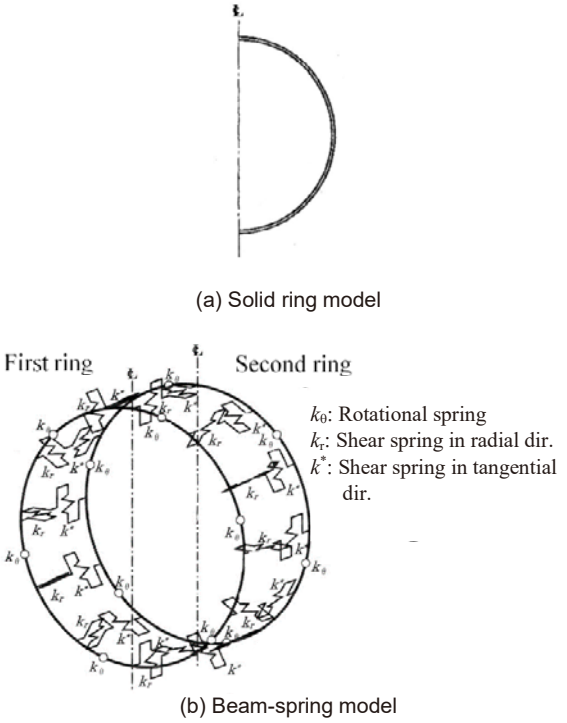

(a) Solid ring model

(b) Beam-spring model

Fig. 2. Schematic drawings of structural model of segmental ring. (JSCE, 2006a)

circumferential directions, respectively; and the ground is represented by ground springs. This model can evaluate the effect of the longitudinal joint and circumferential joint more precisely than the modified usual calculation method, since the bending moment at the longitudinal joint is transferred to the next segments through the circumferential joints as shown in Fig. 3. Therefore, to examine the moment distribution around the tunnel axis in the tunnel axis direction, 3D shell–beam models were developed (Lee et al., 2001; Klappers, 2006; Zheng-Rong et al., 2006; Chub-uppsksrn and Teachaorasinskun, 2010; Oriol and Climent, 2012). These models can calculate a sectional force in the segments, but cannot evaluate ground behaviour around the tunnel.

On the other hand, ground deformation around the

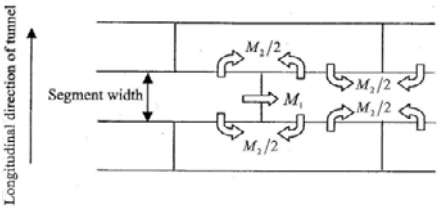

M_0: Design bending moment for main section.
$M_0 = M_1 + M_2$
M_1: Design bending moment for longitudinal joints.
M_2: Bending moment transferred to adjacent rings due to staggered arrangement.

Fig. 3. Transferred bending moment to adjacent rings. (JSCE, 2006a)

tunnel, which causes ground surface settlement and damage to existing neighbouring structures, is an important issue in underground construction. To analyze the ground deformation, it is necessary to model the ground using a continuum model. Consequently, a 2D finite element method (FEM) continuum model with longitudinal joints was developed (Ngoc-Anh et al., 2013). Since, the 2D FEM model is not enough to solve three dimensional problems, especially in case of redistribution of stress (Dias and Kastner, 2012), 3D FEM model has been developed to carry out the analysis on a construction project in details. 3D FEM continuum models without joints were developed (Li et al., 2009; Chakeri et al., 2013). Recently, a 3D FEM continuum model with joints was developed (Ngoc-Anh et al., 2014). Moreover, the behavior of joints in tunnel segment was investigated by 3D FEM analysis (Zili et al., 2014).The 3D FEM model is applied to understand the sectional force of lining and the ground displacement aruond tunnel face during tunnelling (Song et al., 2015).

This paper introduces a 3D FEM continuum model, which can consider longitudinal joints, circumferential joints and non-tension boundary between lining and ground, and validated it by comparing the calculated sectional forces of segmental lining with that by the existing 2D beam spring model (Sugimoto et al., 2011; Lam et al., 2014). Using this model, the effect of the boundary condition at the tunnel end on the sectional force of the segmental lining in the case of staggered building is discussed by taking the number of rings for analysis and the soil stiffness as the parameter.

2. Numerical modeling

2.1 3D FEM model

Figure 4 shows the developed 3D FEM model. Table 1 shows the summary of the element type in this model. The ground was modelled by a solid element. The

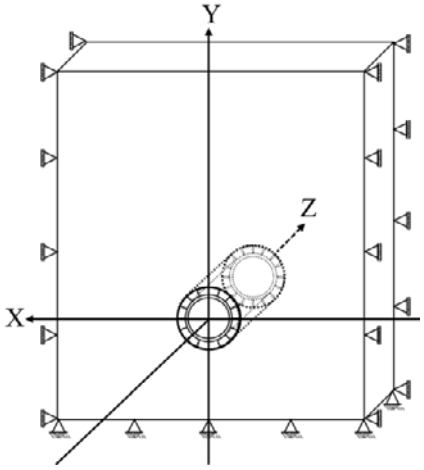

Fig. 4. Boundary condition of 3D FEM model.

Table 1. Element types in a 3D shell–spring model.

Components		Element
Lining		Four nodes isoperimetric curved shell element
Joints	Longitudinal joint	Rotation spring between segments
	Circumferential joint	Translation spring in radial dir. Translation spring in tangential dir. Translation spring in axial dir.
	Surrounding ground	Translation spring in normal dir. Translation spring in tangential dir.

vertical roller was employed as a boundary condition on the sides of the model, and the fixed and free boundary conditions were considered at the bottom and at the top of the model, respectively.

2.2 Shell spring model

The lining model is a 3D shell–spring model as shown in Fig. 5 schematically. The tunnel lining is composed of segmental rings, longitudinal joints and circumferential joints. One ring is composed of eight segments, which were modelled by a shell element. The longitudinal joint was modelled by tying and rotation spring elements. The nodes of the neighbouring segments in a ring, which are assigned at the same coordinates, were connected by tying. The rotation spring generates a moment around the tunnel axis due to the relative rotation of the segments on both sides. The circumferential joint was modelled by translation spring elements in the radial and tangential directions, which is called the shear spring, and by a translation spring element in the tunnel axis direction.

2.3 Interaction between ground and lining

The interaction between segmental lining and ground was modelled by translation spring elements in radial and circumferential directions, which are called touching

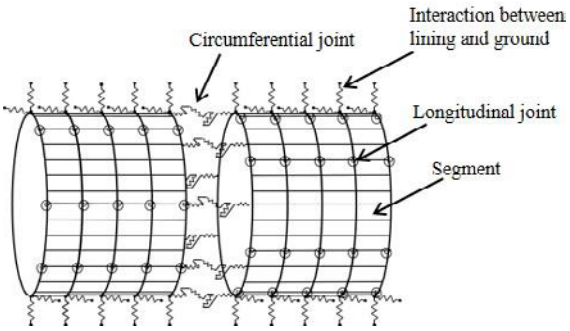

Fig. 5. Schematic 3D shell spring model.

springs. The characteristics of this touching spring were set as shown in Fig. 6, so that the earth pressure in the normal direction against the lining, σ_n, is equal to the earth pressure at rest, σ_{n0}, when the ground displacement in the normal direction, u_n, is equal to zero. This means that σ_{n0} acts on the lining at the start of analysis without deformation. Here, the required displacement to generate σ_{n0} in the touching spring, u_0, is defined as

$$u_0 = \frac{\sigma_{n0}}{k} \quad [1]$$

where *k* is the spring constant of the touching spring.

2.4 Phase analysis

To simulate shield tunnelling, the following three phases are considered:

1. Initial stress analysis: Before excavation, self-weight of the ground is loaded to generate the earth pressure at rest.
2. Tunnel excavation: The soil inside the tunnel is deactivated, and the enforced displacement u_0 is applied to the excavation surface.
3. Installation of the segmental lining: The 3D shell–beam model and the touching spring between the ground and the lining are installed. Fixation on the excavation surface is released, so that the characteristics of the touching spring in Fig. 6 are simulated.

3. Analysis conditions

3.1 Analysis parameters

Table 2 shows the properties of the segmental lining and the ground conditions for the analysis, which were set based on a site data (Sugimoto et al., 2011). The concrete segmental ring has a diameter of 7.87 m, width

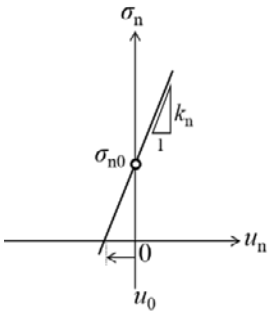

Fig. 6. Characteristics of touching spring.

Table 2. Properties of the segment lining and the ground condition.

Component	Value
Segment	
Radius (m)	3.935
Width (m)	1.000
Height (m)	0.370
Young's modulus (GN/m^2)	33
Poisson's ratio	0.2
Density (kN/m^3)	28.0
Joints	
Segment J. spring const. (MN-m/rad/m)	42.5
Ring J. radial spring const. (MN/m/m)	478
Ring J. tangential spring const. (MN/m/m)	1050
Ring J. axial spring const. (MN/m/m)	173
Ground	
Overburden depth (m)	41.488
Ground water level (m)	GL-11.408
Submerged density (kN/m^3)	5.5
Water density (kN/m^3)	10.0
Coef. of earth pressure at rest K_{H0}	0.5
Coef. of ground reaction k_H (MN/m^3)	10, 100
k_V (MN/m^3)	10, 100
k_t (MN/m^3)	0.001
Touching radial spring const. (MN/m/m)	6181
Touching tangential spring const. (kN/m/m)	0.618

of 1.00 m, and thickness of 0.37 m. Fig. 7 shows the position of the longitudinal joints and circumferential joints in odd number ring and even number ring. The ground was assumed to be one homogeneous layer to simplify the model, since this paper aims to discuss the effect of boundary condition on the obtained sectional force.

To investigate the effect of ground conditions on the sectional force and lining behaviour, the coefficient of subgrade reaction, k_n, was considered as a parameter. From the view point of the ground where shield tunneling method can be applied, the ground with k_n=10 MN/m^3 and 100 MN/m^3 are called "soft ground" and "stiff ground" in this paper (JSCE, 2006a). The following empirical equation (RTRI, 2002) was used as the relationship between Young's modulus of ground in the 3D FEM continuum model, E, and the coefficient of subgrade reaction in the 2D beam spring model, k_n.

$$k_n = 1.58\alpha E B_V^{-0.75} \quad [2]$$

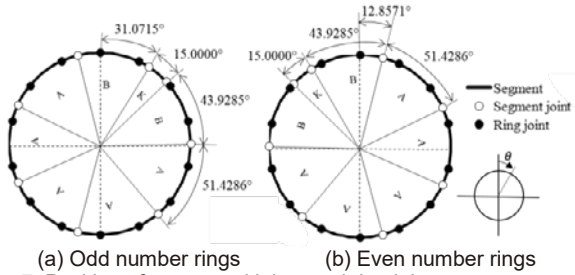

(a) Odd number rings (b) Even number rings

Fig. 7. Position of segmental joints and ring joints.

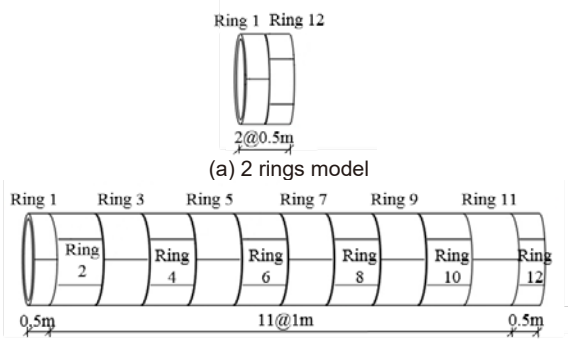

(a) 2 rings model

(b) 12 rings model

Fig. 8. Segmental lining model (staggered building).

$$B_V = 2R_c \quad [3]$$

where α is the factor for the test method of E, B_V is the equivalent diameter of the tunnel, and R_c is the radius of the tunnel.

The sectional force of segmental lining, such as the axial force in the circumferential direction and the bending moment around the tunnel axis, is considered to be affected by the boundary conditions at the tunnel end of the model, since in the case of staggered building of segmental lining, the bending moment around the tunnel axis distributes not only in the circumferential direction but also in the tunnel axis direction as shown in Fig. 3. Therefore, the number of segmental rings in the model is taken as a parameter to examine the effect of staggered building of segmental lining on the sectional force of a segment and the lining behavior. Concretely, the models with 2 and 12 rings are used as shown in Fig. 8.

Table 3 shows the analysis cases in this study. Here, the segments with half a width are used at both ends of the lining, so that the effects of the circumferential joint and the external loads acting on the segments are similar at both the tunnel end and the tunnel center.

3.2 Analysis model

Figure 9 shows the 3D FEM mesh for this analysis. To eliminate the influence of the boundary at the bottom of the model and the sidewall parallel to the tunnel axis, the mesh model was generated, as the width of the

Table 3. Analysis cases.

Case	No. of ring	k_n (MN/m^3)
11	12 rings	10
12	12 rings	100
21	2 rings	10
22	2 rings	100

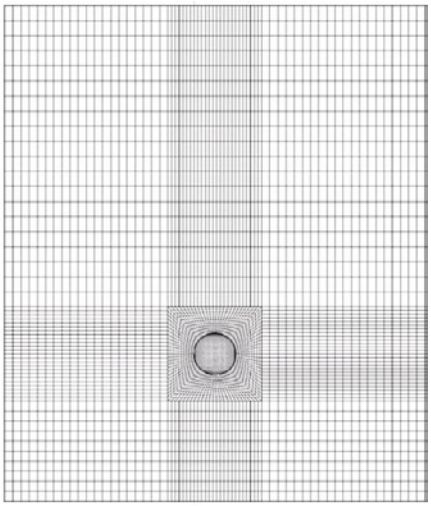

Fig. 9. 3D FEM mesh.

model is about nine times the tunnel diameter, and the depth of the model under the tunnel is about three times the tunnel diameter (JSCE, 2006b). The segmental lining was divided into 100 elements in the circumferential direction and was modelled by the isoparametric curved shell elements with four nodes. Furthermore, the segmental lining width of 1m were divided by four, that is, the interval of the node is 0.25m, which is equivalent to the interval of the nodes in the circumferential directions. The ground was modelled by the isoparametric solid element with eight nodes.

4. Results and discussions

4.1 Validation with existing model

The concept on the interaction between ground and lining of the proposed 3D FEM continuum model is different from that of the existing 3D FEM model (e.g. (JSCE, 2006b). Therefore, to validate this 3D FEM continuum model, the sectional forces of lining by this model were compared with those by the 2D beam spring model (Sugimoto et al., 2011; Lam et al., 2014), because 1) as for the interaction between ground and lining, the 2D beam spring model has the same concept as this model; 2) the influence of that interaction appears mostly at the sectional forces of lining; and 3) the 2D beam spring model has been validated using the site data as

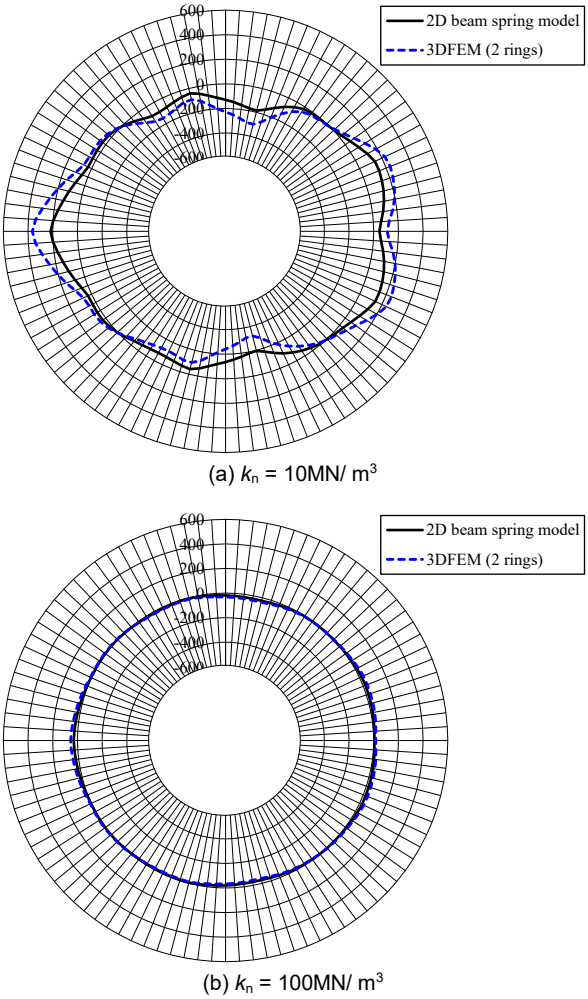

(a) k_n = 10MN/ m^3

(b) k_n = 100MN/ m^3

Fig. 10. Bending moment around tunnel axis (Ring 1). (kN-m/m)

shown in Table 2. It is noted that the sectional force using in this section is the total one in one ring, to compare the sectional force by the 3D FEM continuum model with that by the 2D beam spring model.

Figures 10, 11, and 12 show the bending moment around tunnel axis, M, the axial force in circumferential direction, N, and the normal displacement of segment, u_n, respectively, at Ring 1 calculated by both models with k_n=10 MN/m^3 and 100 MN/m^3. From these figures, the following were found:

1. In the case of k_n=10 MN/m^3 (soft ground), the shapes of the calculated M distribution by both models are flat in the horizontal direction and almost similar tendency, that is, the calculated M fluctuates according to the position of the longitudinal joint, but the shape of the calculated M distribution by the 3D FEM continuum model is a little bit flatter in the horizontal direction than that by the 2D beam spring model.

2. In the case of k_n=100 MN/m^3 (stiff ground), the shapes of the calculated M distribution by both models are circular and their values are close to zero.

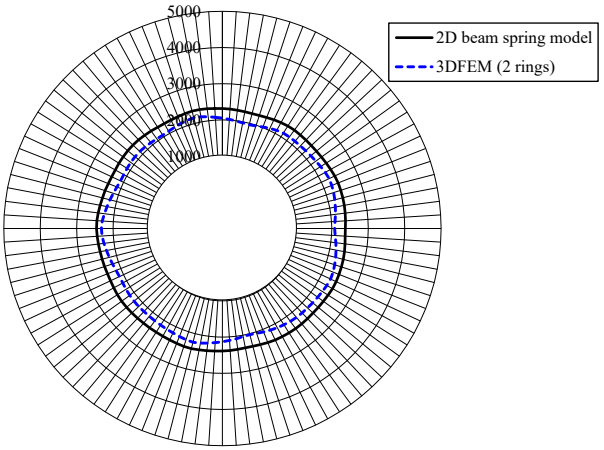

(a) k_n = 10MN/ m^3

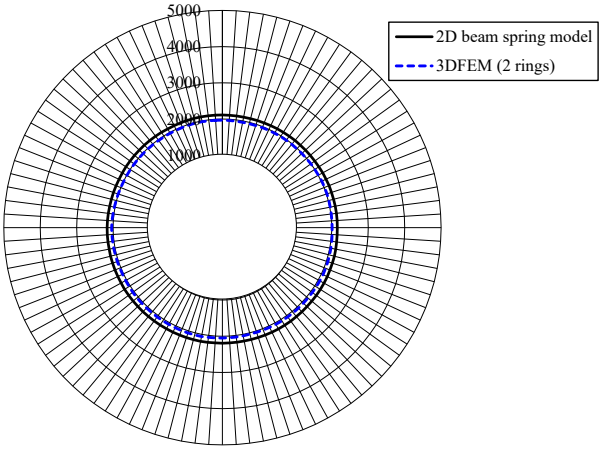

(b) k_n = 100MN/ m^3

Fig. 11. Axial force in circumferential direction (Ring 1). (kN/m)

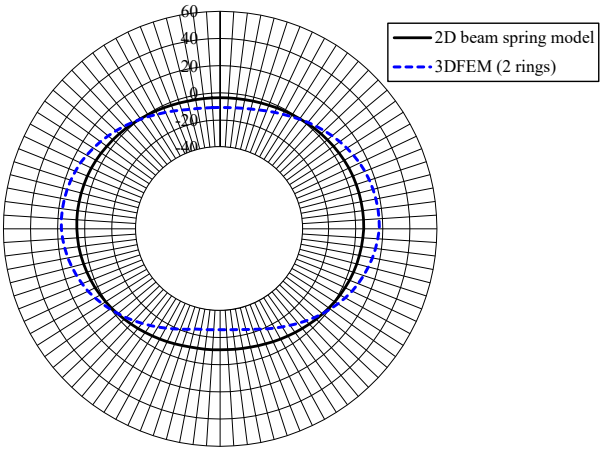

(a) k_n = 10MN/ m^3

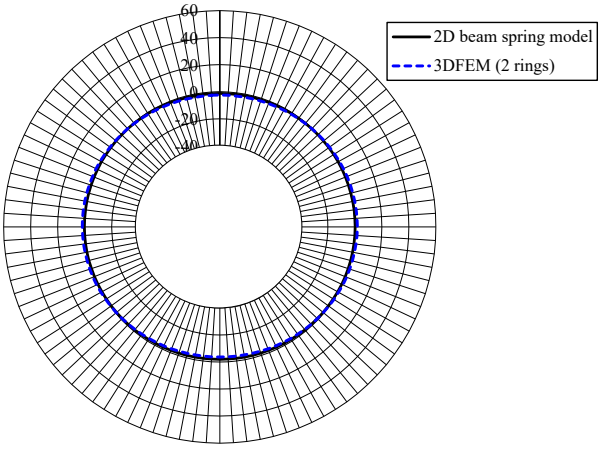

(b) k_n = 100MN/ m^3

Fig. 12. Normal displacement of segment (Ring 1). (mm)

3. The calculated *N* distributions by both models are a circular shape, but the *N* by the 3D FEM continuum model is a little bit smaller than that by the 2D beam spring model.

4. The calculated *N* with k_n=10 MN/m^3 is a little bit larger than that with k_n=100 MN/m^3 for both models. The calculated *N* with k_n=10 MN/m^3 fluctuates along the circumferential direction, while that with k_n=100 MN/m^3 are almost constant.

These can be explained as follows:

1. In the case of the 3D FEM continuum model, the deformation of the lining is larger (Fig. 12), and the shape of the bending moment distribution, *M*, is flatter in the horizontal direction (Fig. 10), especially with k_n=10 MN/m^3, compared with the 2D beam spring model, since the 3D FEM continuum model can consider the ground movement around tunnel and the redistribution of stress due to ground, while the 2D beam spring model can not consider them. Furthermore, the axial force, *N*, by the 3D FEM continuum model is smaller than that by the 2D beam spring model, since the ground movement around tunnel corresponding to the ground reaction force makes the ground reaction force acting on the lining decrease, in the case of the 3D FEM continuum model.

2. In the case of k_n=100 MN/m^3, the deformation of the lining is smaller (Fig. 12), and the shape of the bending moment distribution, *M*, is more circular and close to zero (Fig. 10), since the ground reaction force is generated with smaller displacement, compared with those with k_n=10 MN/m^3. Furthermore, the axial force, *N*, with k_n=100 MN/m^3 is a little bit smaller than that with k_n=10 MN/m^3, since lining shrinks due to hydraulic water pressure (Sugimoto et al., 2011), and it makes the ground reaction force acting on the lining decrease more, in the case of k_n=100 MN/m^3.

3. According to the above examination, in the case of k_n=100 MN/m^3, it was confirmed that the 3D FEM continuum model provides the almost same sectional forces of the lining as the 2D beam spring model by using Eqs. (2) and (3). This is because the interaction condition between ground and lining is almost same at both models, that is, the excavation surface displacement in the 3D FEM continuum model is very small as shown in Fig. 12, which coincides with the fixed support at the

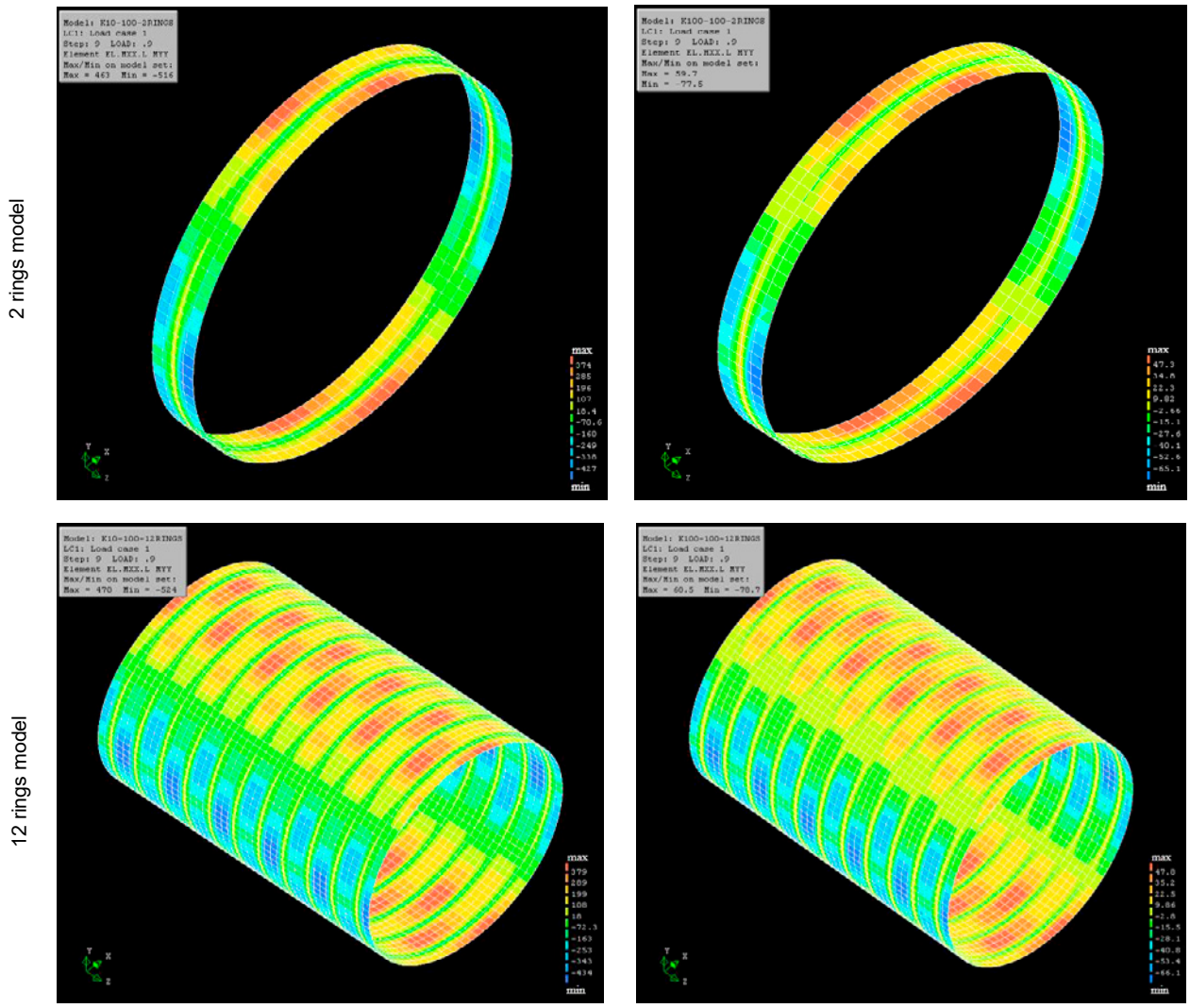

(a) k_n = 10MN/ m^3 (b) k_n = 100MN/ m^3

Fig. 13. Bending moment around tunnel axis. (kN-m/m)

excavation surface in the 2D beam spring model. On the other hand, in the case of k_n=10 MN/m^3, the calculated sectional forces of the lining were different between both models. This is because the interaction condition between ground and lining, which is affected by the excavation surface displacement as shown in Fig. 12, is different between both models. From the viewpoint of mechanism, it is considered to be more reasonable that the ground movement around tunnel, which can be represented by only the 3D FEM continuum model, is allowed. Therefore, in the case of soft ground, it is expected to get a good fitting of sectional forces by both models, if the proper relationship between Young's modulus of ground in the 3D FEM continuum model, E, and the coefficient of subgrade reaction in the 2D beam spring model, k_n is established, instead of Eqs. (2) and (3). Therefore, the proposed 3D FEM continuum model is considered to provide reasonable results.

4.2 Bending moment

The contours of the calculated bending moment of the lining around tunnel axis, M, with k_n=10 MN/m^3 and 100 MN/m^3, are shown in Fig. 13. From these figures, the followings were found:

1. The shape of the bending moment distribution becomes flat in the horizontal direction in the case of soft ground. This indicates that the normal earth pressure σ_n at the top and the bottom is larger than σ_n at the spring line since the coefficient of earth pressure at rest K_0 is 0.5.

2. The bending moment distribution is different between the odd number ring and the even number ring. This difference comes from the effect of staggered building of segmental lining as shown in Fig. 3.

Figure 14 shows the calculated bending moment of

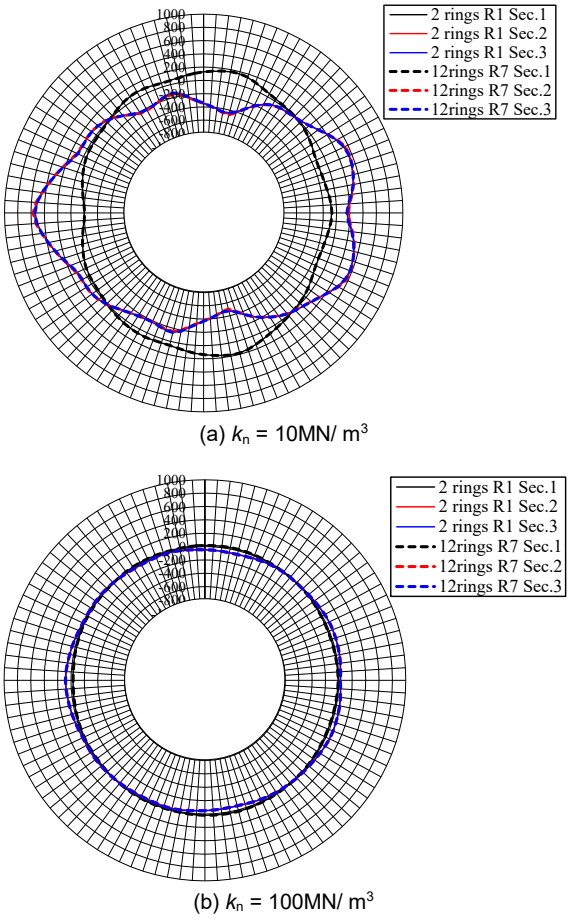

(a) k_n = 10MN/ m^3

(b) k_n = 100MN/ m^3

Fig. 14. Bending moment around tunnel axis. (kN-m/m)

lining, *M*, at Ring 1 of the 2-ring model and Ring 7 of the 12-ring model with k_n=10 MN/m^3 and 100 MN/m^3. Since the ring model consists of four shell elements in width, Sec. 1 and Sec. 3 are the cross-sections at the end and at the center of the ring, respectively. Sec. 2 is the cross-section at the middle between Sec. 1 and Sec. 3. From these figures, the followings were found:

1. The bending moment *M* in Sec. 3 (the center section of the ring) fluctuates more than the *M* in Sec. 1 (the end section of the ring). This indicates that *M* at the boundary between the two rings is levelled, since *M* transfers to the next ring through the circumferential joints.

2. The *M* at Ring 1 of the 2-ring model agrees well with that at Ring 7 of the 12-ring model for both soft and stiff ground. The difference between the 2-ring model and the 12-ring model is less than 1% against the absolute *M* for both k_n=10 MN/m^3 and 100 MN/m^3. This indicates that the boundary condition does not significantly affect the bending moment for both soft and stiff ground.

3. The absolute value of *M* in the soft ground is larger than that in the stiff ground, since the deformation of the lining is limited due to the higher ground reaction force in the case of stiff ground.

4.3 Axial force

Figure 15 shows the contours of the calculated axial force in the circumference direction, *N*, with k_n=10 MN/m^3 and 100 MN/m^3. From these figures, the followings were found:

1. The axial force *N* at the crown and at the invert is smaller than the *N* at the spring lines.

2. The axial force distribution is different between the odd number ring and the even number ring. This difference comes from the effect of the staggered building of segmental lining.

Figure 16 shows the axial force of lining, *N*, at Ring 1 of the 2-rings model, Ring 1 of the 12-ring model, and Ring 7 of the 12-ring model with k_n=10 MN/m^3 and 100 MN/m^3. From these figures, the followings were found:

1. In the case of the soft ground, the *N* in Sec. 3 (the center section of the ring) fluctuates more than the *N* in Sec. 1 (the end section of the ring). This indicates that *N* at the boundary between two rings is levelled, since *N* transfers to the next ring through the circumferential joints.

2. In the case of the soft ground, the *N* distributions at the end of the model (i.e., Ring 1 of the 2-ring model and Ring 1 of the 12-ring model) are almost same. However, the *N* at the center of the model (i.e., Ring 7 of the 12-ring model), where the effect of the boundary condition is expected to be neglected, fluctuates less than the *N* at the end of the model, especially in Sec. 3. The *N* at the end of the model is larger than the *N* at the center of the model with about 7.0% of the maximum axial force *N*. In Sec. 1, the fluctuation of *N* decreases according to the order of Ring 1 of the 2-ring model, Ring 1 of the 12-ring model, and Ring 7 of the 12-ring model. This order is considered to be same as that of the effect of the boundary condition. In Sec. 2, the *N* distribution is almost same among the three combinations of the number of rings and the ring position. The difference is less than 1.0% of the maximum axial force *N*. This finding indicates that the boundary condition affects the axial force in the case of the soft ground.

3. In the case of the stiff ground, the *N* distribution among the three combinations of the number of rings and the ring position is a circular shape and almost same in each section.

Table 4 shows the theoretical and calculated axial forces at the spring line by the 2-ring model. The theoretical axial force is obtained from the overburden load and the self-weight of the segment. In this table, "diff" is the different rate of the calculated *N* from the theoretical *N*. From this table, the followings were found:

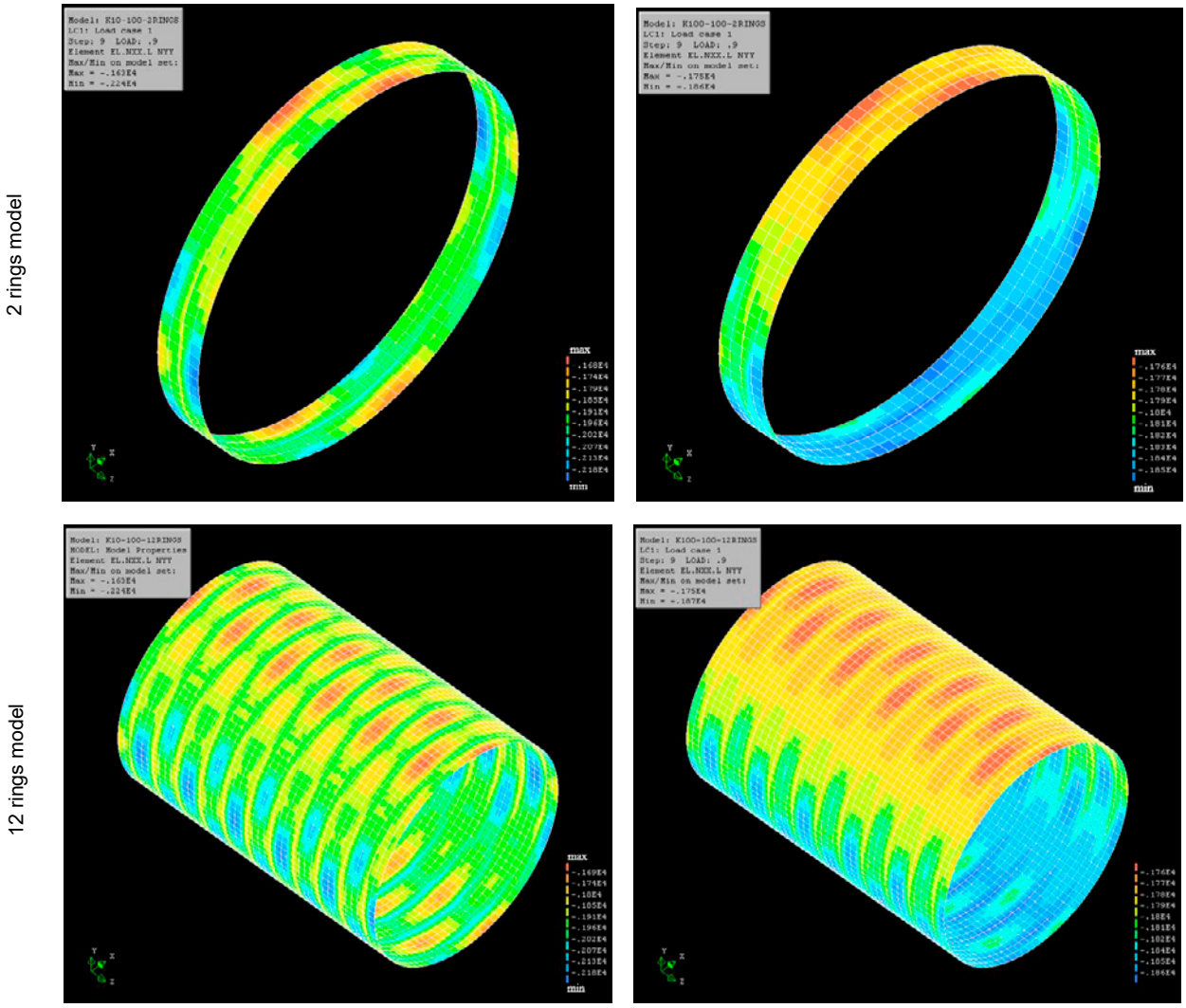

(a) k_n = 10MN/ m^3 (b) k_n = 100MN/ m^3

Fig. 15. Axial force in circumference direction. (kN/m)

1. The calculated *N* values at Rings 1 and 2 of "Right SL" coincide with those at Rings 2 and 1 of "Left SL", respectively. The average of the calculated *N* at "Right SL" and "Left SL" is almost same. This comes from the different position of the longitudinal joints in the case of staggered building of segment lining.

2. The calculated *N* decreases at about 16.7% with k_n=10 MN/m^3 and at about 23.4% with k_n=100 MN/m^3 from the theoretical *N*. This comes from the followings: 1) The touching spring model has non-tension characteristics, as shown in Fig. 6, which allow the active side earth pressure; and 2) In the active state, the earth pressure drops more in the case of stiff ground than in soft ground.

Table 4. Axial force at the spring line.

Position		Theoretical N (kN/m)	k_n=10 MN/m^3 Cal N (kN/m)	diff. %	k_n=100 MN/m^3 Cal N (kN/m)	diff. %
Right SL	Ring1	2643	2303	-12.9	2034	-23.0
	Ring2		2095	-20.7	2009	-24.0
	Ave.		2199	-16.8	2021	-23.5
Left SL	Ring1	2643	2100	-20.5	2014	-23.8
	Ring2		2308	-12.7	2039	-22.8
	Ave.		2204	-16.6	2027	-23.3

4.4 Circumferential joint

Figure 17 shows the axial force of the tangential spring, radial spring, and tunnel axis spring, respectively, at the circumferential joints. From these figures, the followings were found:

1. The axial forces in the tangential spring, N_t, has a relation with the axial forces in the segmental ring in the circumferential direction in Sec. 1 (the end section of a ring). The N_t with k_n=10 MN/m^3 fluctuates more than the N_t with k_n=100 MN/m^3. At k_n=10 MN/m^3, the fluctuation

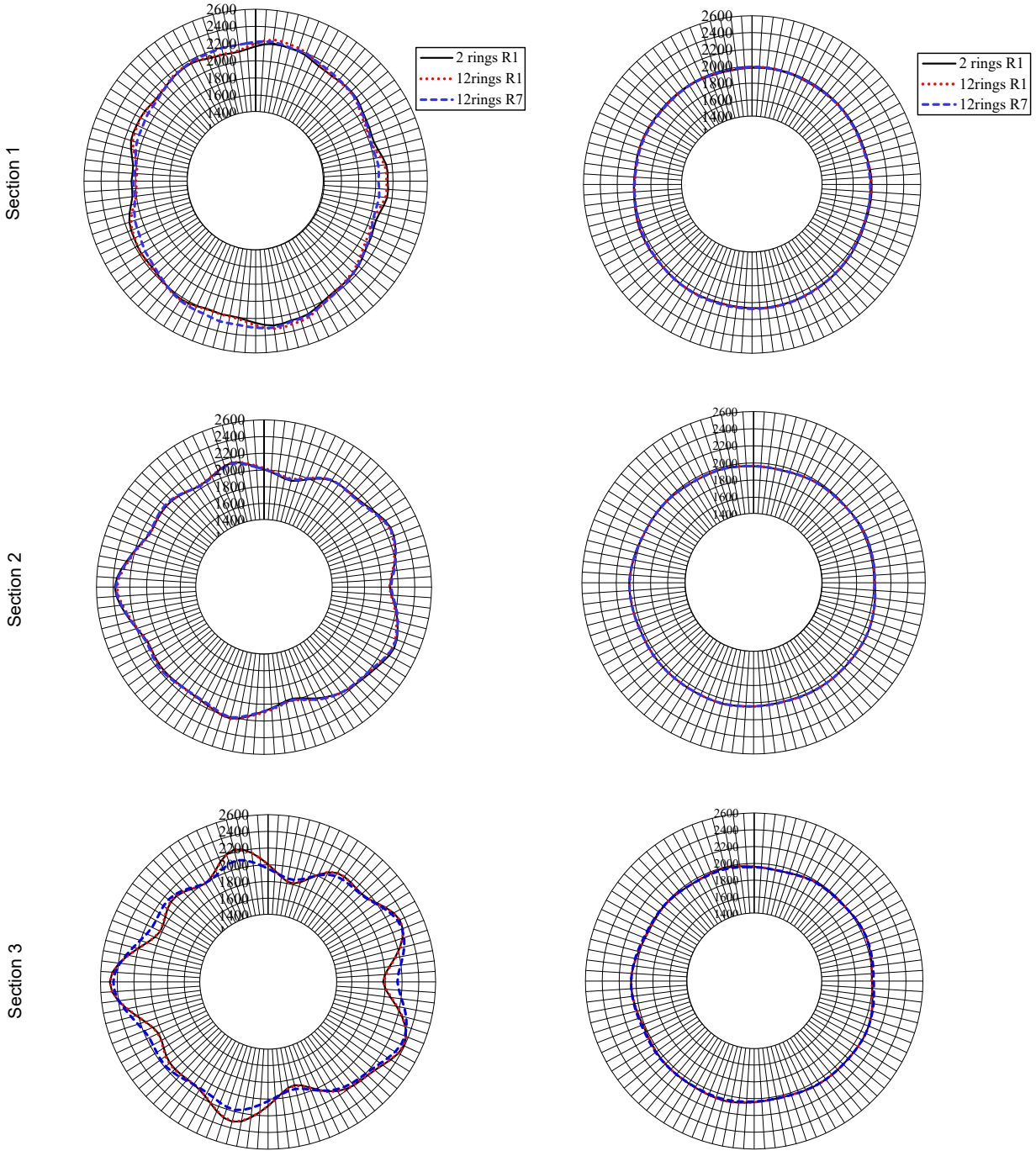

(a) k_n = 10MN/ m^3 (b) k_n = 100MN/ m^3

Fig. 16. Axial force in circumference direction at each section. (kN/m)

decreases in the order of Rings 1 and 2 of the 2-ring model, Rings 1 and 2 of the 12-ring model, and Rings 7 and 8 of the 12-ring model. These can be explained as the same as the *N* distribution in a ring.

2. The axial forces in the radial spring, N_r, has a relation with the bending moment of the segmental ring around the tunnel axis in Sec. 1 (the end section of a ring). The N_r with k_n=10 MN/m^3 fluctuates at the longitudinal joints of both side segments, but the N_r with k_n=100 MN/m^3 is close to 0 except for the longitudinal joint positions. The N_r distribution does not depend on the number of rings and the ring position. These can be explained as the same as the *M* distribution in a ring.

3. The axial forces in the axial spring, N_a, is almost

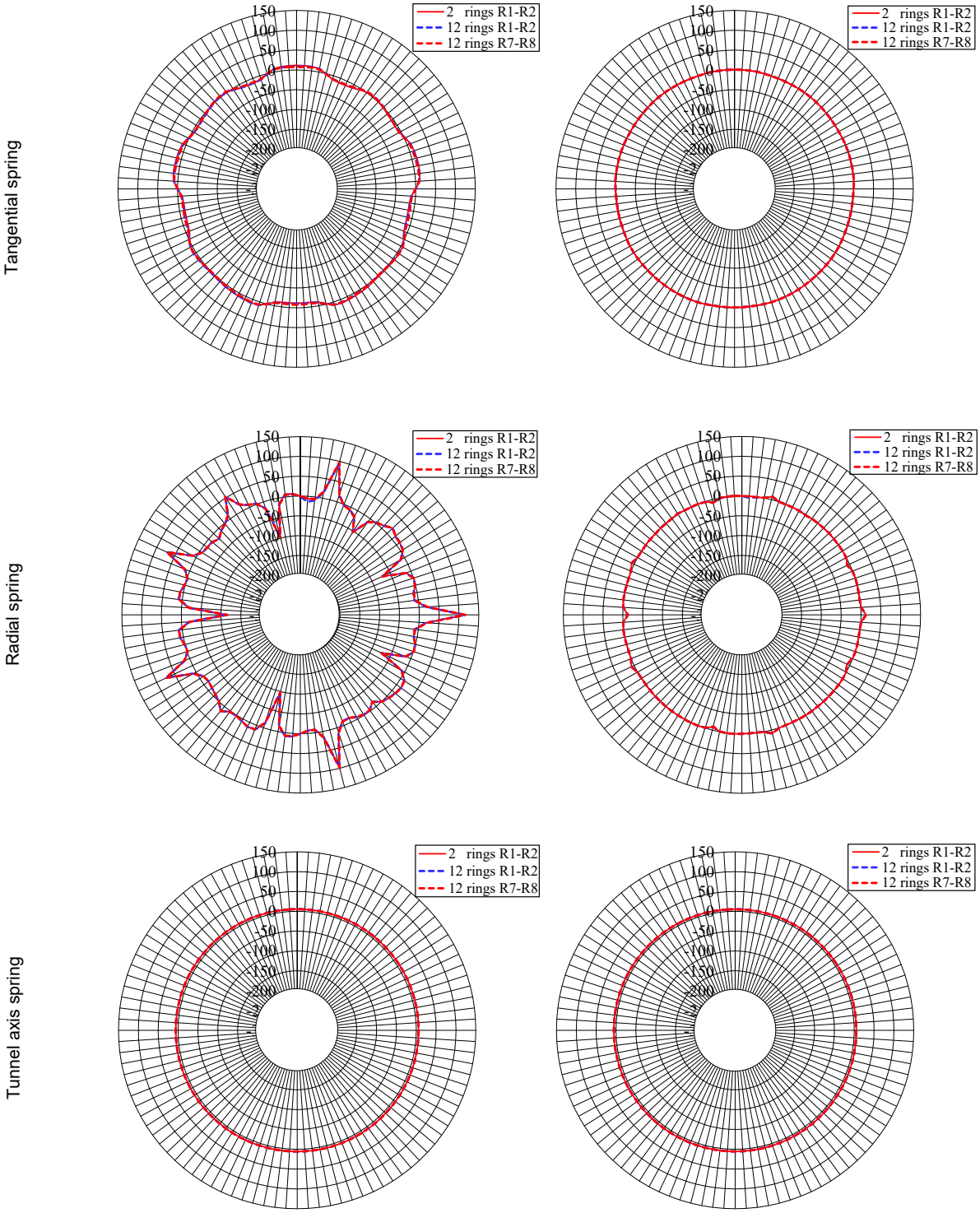

(a) k_n = 10MN/ m^3 (b) k_n = 100MN/ m^3

Fig. 17. Axial force of spring at ring joint. (kN/m)

constant for both k_n=10 MN/m^3 and 100 MN/m^3, and does not depend on the number of rings and the ring position. Accordingly, the state of this model is close to the 2D plain strain condition.

4.5 Segment displacement

Figure 18 shows the average of the normal segment displacement against the lining surface, u_n, (+: outward of

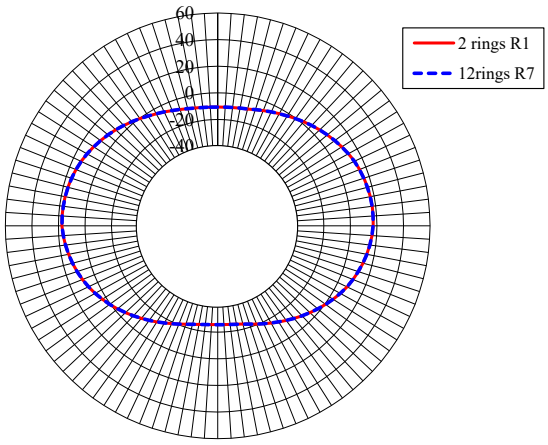

(a) k_n = 10MN/ m^3

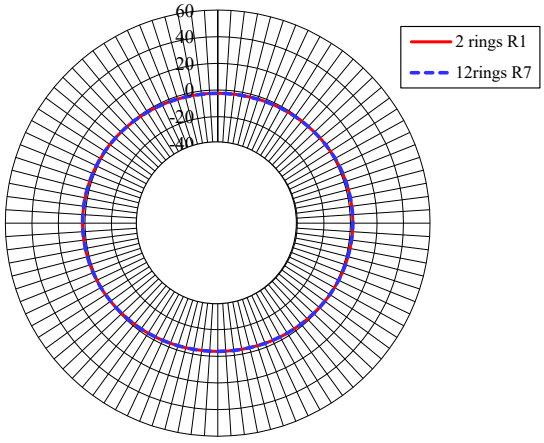

(b) k_n = 100MN/ m^3

Fig. 18. Normal displacement of segment. (mm)

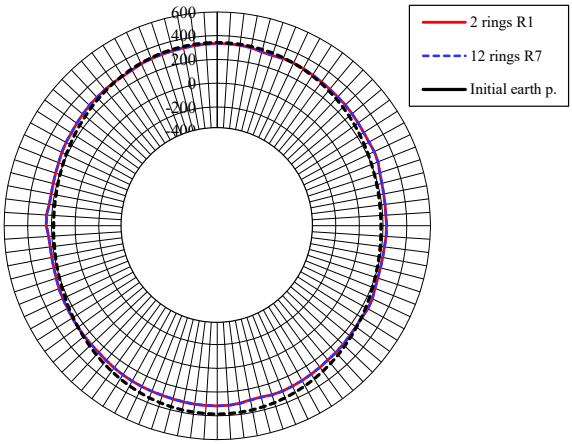

(a) k_n =10MN/ m^3

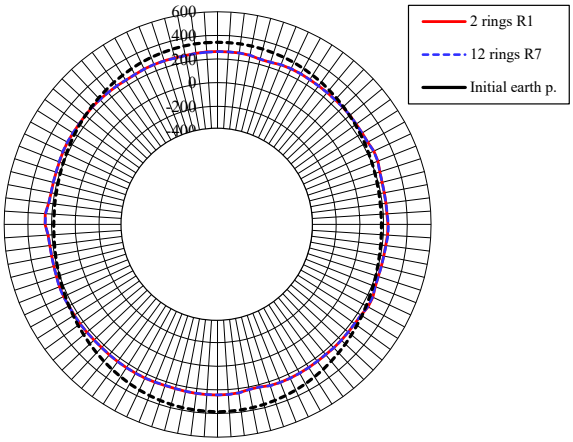

(b) k_n =100MN/ m^3

Fig. 19. Normal effective earth pressure. (kPa)

tunnel) in a ring with k_n=10 MN/m^3 and 100 MN/m^3. From these figures, the followings were found:

1. The shape of the segment deformation of the ring at k_n=10 MN/m^3 becomes flat in the horizontal direction, while that at k_n=100 MN/m^3 is close to circular. This is because u_n decreases to generate a certain ground reaction force as k_n increases.
2. The ring is lifted upward due to buoyancy.
3. The u_n at Ring 1 of the 2-ring model is close to that at Ring 7 of the 12-ring model.

4.6 Normal earth pressure

Figure 19 shows the average of the normal effective earth pressure, σ_n', in a ring with k_n=10 MN/m^3 and 100 MN/m^3. From these figures, the followings were found:

1. The shape of the σ_n' distribution is more circular than that of the initial normal effective earth pressure, σ_{no}'. This comes from the redistribution of σ_{no}' due to the stiffness of the ground and the segmental lining.
2. The shape of the σ_n' distribution with k_n=100 MN/m^3 is more circular than that with k_n=10 MN/m^3. This can be explained as the same as u_n distribution.
3. The σ_n' at Ring 1 of the 2-ring model is close to that at Ring 7 of the 12-ring model.

5. Conclusions

This study developed a 3D FEM continuum model with longitudinal joints, circumferential joints, and non-tension boundary between ground and lining, and validated the developed 3D FEM continuum model, comparing the calculated section forc es by this model with those by the existing 2D beam spring model. Furthermore, the lining behaviour is simulated by its model to confirm the effect of the boundary condition at the tunnel end on segmental lining behaviour in the case of staggered building. The following conclusions can be made:

1. Even in the case of staggered building, the boundary condition at the tunnel end generally does not have a significant effect on the sectional force for both soft and stiff grounds, except for the axial force in the case of soft ground. Since the difference in the axial force between the 2-ring model and the 12-ring model is only 7% of the maximum axial force, and the 2-ring model provides the safe side results from the viewpoint of segment design, the 2-ring model can be used as the developed 3D FEM continuum model.

2. The effect of the boundary condition at the tunnel end and the ground stiffness on the sectional force and the lining behaviour was examined. Finally, it was confirmed that the obtained results are reasonable from the viewpoint of mechanism.

As a future research, it is recommended to clarify the mechanism in the difference between the 2-ring model and the 12-ring model and to validate the proposed model using a site data on the ground movement around tunnel.

References

Chakeri, H., Ozcelik, Y., and Unver, B., 2013. Effects of important factors on surface settlement prediction for metro tunnel excavated by EPB. Tunnelling and Underground Space Technology, **36**: 14–23.

Chub-uppsksrn, S., and Teachaorasinskun, T., 2010. Influence of segmental joints on tunnel lining. Tunnelling and Underground Space Technology, **25** (4): 490–494.

Dias, D., and Kastner, R., 2012. Movements caused by the excavation of tunnels using face pressurized shield-analysis of monitoring and numerical modelling results. J. Engineering Geology, **152**: 17-25.

ITA working group no. 2., International Tunnelling Association., 2000. Guidelines for the design of shield tunnel lining. J. Tunnelling and Underground Space Technology,**15** (3): 303-331.

Japan Society of Civil Engineers (JSCE), 1996. Standard Specification for Shield Tunneling Method. JSCE.

Japan Society of Civil Engineers (JSCE), 2006a. Standard Specification for Tunneling-2006: Shield Tunnels. JSCE.

Japan Society of Civil Engineers (JSCE), 2006b. Tunnel library 16, Model experiments and numerical analyses in mountain tunnelling. JSCE.

JTA., 2000.Step up seminar on shield tunnelling. JTA. (in Japanese)

Klappers, C., Grübl, F., and Ostermeier, B., 2006. Structural analyses of segmental lining – coupled beam and spring analyses versus 3D-FEM calculations with shell elements. Proc. of World Tunnel Congress 2016. ITA.

Lam, L.G., Thi, H.N., Sugimoto, M., Hino, T., and Bergado, D.T., 2014. Numerical Modeling Involving Backfill Grouting Effects for Segmental Tunnel. Proceeding of the 9th International Symposium on Lowland Technology, Saga, Japan.

Lee, K.M., Hou, X.Y., Ge, X.W., and Tang, Y., 2001. An analytical solution for a jointed shield-driven tunnel lining. Int. J. Numer. Anal. Meth. Geomech, **25**: 365-390.

Li, Y., Emeriault, F., Kastner, R., and Zhang, Z.X., 2009. Stability analysis of large slurry shield-driven tunnel in soft clay. Tunnelling and Underground Space Technology, **24**: 472–481.

Murakami, H. and Koizumi, A., 1978. Study on load bearing capacity and mechanics of shield segment ring. J. Japan Society of Civil Engineering, **272**: 103-115. (in Japanese)

Ngoc-Anh, D., Daniel, D., Pierpaolo, O., and Irini, D. M., 2013. 2D numerical investigation of segmental tunnel lining behavior. Tunnelling and Underground Space Technology, **37**: 115–127.

Ngoc-Anh, D., Daniel, D., Pierpaolo, O., and Irini, D. M., 2014. Three-dimensional numerical simulation for mechanized tunnelling in soft ground: the influence of the joint pattern. J. Acta Geotechnica, **9** (4): 673-694.

Oriol, A., and Climent, M., 2012. Three dimensional structural response of segmental tunnel linings. Engineering Structures, **44**: 210–221.

Railway Technical Research Institute (RTRI)., 2002. Design Standards for Railway Structures and Commentary (Urban Mountain Tunnel). RTRI. (in Japanese)

Song, J., Miao, L., and Feng, S., 2015. The effect of water boundary conditions of advance face and lining on the evolution of internal force in lining. Lowland Technology International, **17** (1): 1-10.

Sugimoto, M., Sramoon, A., and Okazaki, M., 2011. Tunnel lining design method by frame structure analysis using ground reaction curve. J. Japan Society of Civil Engineering, **67** (1): 61-77. (in Japanese)

Zheng-Rong, H., Wei, Z., Jing-Hua, L., Jan, L. and Rui, L., 2006. Three dimensional numerical modelling of shield tunnel lining. J. Tunnelling and Underground Space Technology, **21**(3-4): 434-434.

Zili, Li., Kenichi, S., Fei, W., Peter, W., and Kiwamu, T., 2014. Behaviour of cast-iron tunnel segmental joint from the 3D FE analyses and development of a new bolt-spring model. Tunnelling and Underground Space Technology, **41**:176-192

Symbols and abbreviations

u	Displacement
u_n	Displacement from the initial excavation surface to the lining surface
u_0	Enforced displacement of excavation surface
α	The factor for the test method
k	Spring constant
k_n	Coefficient of subgrade reaction
E	Young's modulus
B_V	Diameter of tunnel
R_c	Radius of tunnel
σ_n	Normal earth pressure
σ_{n0}	Initial normal earth pressure
M	Bending moment of tunnel lining
N	Axial force of tunnel lining
N_a	Axial force of axial spring at circumferential joint
N_r	Axial force of radial spring at circumferential joint
N_t	Axial force of tangential spring at circumferential joint